Available online at www.sciencedirect.com

ScienceDirect

Procedia Manufacturing 38 (2019) 1244–1251

Procedia MANUFACTURING

www.elsevier.com/locate/procedia

29th International Conference on Flexible Automation and Intelligent Manufacturing (FAIM2019), June 24-28, 2019, Limerick, Ireland.

Effect of material hybridization on the strength of scarf adhesive joints

D.L. Alves[a], R.D.S.G. Campilho[a,b,*], R.D.F. Moreira[a], F.J.G. Silva[a], M.G. Cardoso[a]

[a]*ISEP-School of Engineering, Rua Dr. António Bernardino de Almeida 431, 4200-072 Porto, Portugal*
[b]*INEGI, Campus da FEUP, Rua Dr. Roberto Frias 400, 4200-465 Porto, Portugal*

Abstract

Adhesively-bonded joints have become more efficient due to the improvement of adhesives' characteristics. On the other hand, with the use of composites in structures it is possible to reduce weight. Due to this, new techniques are being explored, including adhesively-bonding different materials. Nowadays, in many high performance structures, it is necessary to combine composite materials with other light-weighted metals such as aluminium or titanium. This work reports on an experimental and numerical study for hybrid scarf joints between composite and aluminium adherends, and considering different values of the scarf angle (α). The numerical analysis by Finite Elements (FE), using the software Abaqus®, enabled the obtainment of peel (σ_y) and shear stresses (τ_{xy}), which are then used to discuss the strength between different joint configurations. Cohesive zone modelling (CZM) was used to predict the joint strength and the results were compared to the experiments for validation. The joints' behaviour was highly dependent on α, and CZM were validated for the design process of hybrid scarf joints.

Keywords: Cohesive Zone Models; Structural Adhesive; Hybrid Joints: Scarf Joints.

1. Introduction

As a result of the mechanical characteristics improvements of adhesives, adhesive bonding is progressively replacing traditional joining methods such as bolting or riveting [1]. In recent years, the many advances made in the

* Corresponding author. Tel.: +351-939526892; fax: +351-228321159.
E-mail address: raulcampilho@gmail.com

10.1016/j.promfg.2020.01.216

manufacturing of composite materials, resulting in production costs' reduction and continuous manufacturing, turned them possible to be used in the commercial automotive industry, instead of restricting them to highly demanding industries as it occurred in the past. With the use of composites, it is possible to reduce the vehicle weight, which is a very important issue for automotive manufacturers, allowing to increase the vehicles' performance and also reducing the fuel consumption [2]. Due to this, new joining techniques are being developed, such as hybrid adhesively-bonded joints, which consist of bonding different materials, or on the combination of traditional joining technics, such as bolting or riveting together with the use of a structural adhesive. Nowadays, in many high performance structures, it is necessary to combine composite materials with other light-weighted metals such as aluminium or titanium, for the purpose of structural optimization, e.g. as detailed by Graham et al. [3].

It is possible to use several joint configurations depending on the application. The single-lap joint is undoubtedly one of the most used joint configurations due to its fabrication simplicity and non-necessity of any particular manufacturing skills. Although its geometry is rather simple, the resulting σ_y and τ_{xy} stress distributions in the adhesive layer are highly complex. More common joint configurations are double-lap, stepped and scarf joints. Scarf joints are very interesting because, unlike single-lap joints, they do not cause bending of the adherends, which negatively influences the joints' strength [4], and this is the reason why scarf-bonded joints are increasingly being used in industrial applications. However, the mechanical strength of scarf joints is still affected by the over stresses near the edges of the adhesive layer although, when compared to single and double-lap joints, they are much smaller.

Many studies have been made in adhesive bonding techniques to join dissimilar materials, like the work of Afendi et al. [5], in which the strength of adhesively-bonded scarf joints between dissimilar materials, and bonded with an epoxy adhesive, are predicted. The mechanical tests between dissimilar adherends (steel and aluminium alloy) were conducted under a remote tension load considering different values of α and adhesive thickness (t_A), which originated different failure loads. The authors concluded through a FE analysis that a stress singularity exists at the steel/adhesive interface tip of the joint, which was also confirmed by failure surface observations showing that failure always initiated at this point. In the work of Yelpale et al. [6], the tensile strength of adhesively-bonded scarf joints was experimentally and numerically obtained for various scarf angles. A commercially available epoxy-based adhesive was used to bond a glass-epoxy composite to Bakelite adherends, therefore originating a hybrid joint. The authors concluded that the maximum strength was obtained for α=30º, that the increase of α caused a strength reduction, and also that the strength of scarf adhesive joints with glass epoxy adherends is higher than that with Bakelite adherends.

This work reports on an experimental and numerical study for hybrid scarf joints between composite and aluminium adherends, and considering different values of the scarf angle. The numerical analysis by FE, using the software Abaqus®, enabled the obtainment of σ_y and τ_{xy} stresses which are then used to discuss the strength between different joint configurations. CZM were used to predict the joint strength and the results were compared to the experiments for validation.

2. Experimental work

The AW6082 T651 high strength aluminium alloy and a unidirectional Carbon Fibre Reinforced Plastic (CFRP) composite were selected as the adherend material. The stress-strain (σ-ε) curves of the aluminium alloy were obtained as described in the standard ASTM-E8M-04 [7]. The evaluated mechanical properties are as follows: Young's modulus (E) of 70.07±0.83 GPa, tensile yield stress (σ_e) of 261.67±7.65 MPa, tensile strength (σ_f) of 324.00±0.16 MPa and tensile failure strain (ε_f) of 21.70±4.24% [8]. The CFRP composite has a unit ply thickness of 0.15 mm. The laminates were produced by the hand lay-up technique with 20 layers, equally oriented, and then cured following the manufacturer's parameters in a hot plates press. In the simulations, the laminates were treated as elastic orthotropic, with the elastic constants given in reference [9]. The ductile epoxy adhesive Araldite® 2015, evaluated in this work, was previously characterized regarding the required mechanical and fracture properties [8, 10]. The mechanical properties in tension (E, σ_e, σ_f and ε_f) were found by bulk dogbone specimens, fabricated as specified in the Standard NF T 76-142. Furthermore, thick adherend shear tests were performed to estimate the shear mechanical properties. σ_e and the shear yield stress (τ_e) were calculated for a plastic strain of 0.2% in the respective curves. The tensile toughness (G_{IC}) and shear toughness (G_{IIC}) estimation was accomplished by Double-Cantilever Beam (DCB) and End-Notched Flexure (ENF) tests, respectively, using robust data reduction schemes. Details of the fabrication process can be found in a former work [11]. The obtained properties are presented in Table 1.

Table 1 – Properties of the adhesive Araldite® 2015 [8, 10, 12].

Property	2015
Young's modulus, E [GPa]	1.85±0.21
Poisson's ratio, ν	0.33 [a]
Tensile yield stress, σ_y [MPa]	12.63±0.61
Tensile strength, σ_f [MPa]	21.63±1.61
Tensile failure strain, ε_f [%]	4.77±0.15
Shear modulus, G [GPa]	0.70 [b]
Shear yield stress, τ_y [MPa]	14.6±1.3
Shear strength, τ_f [MPa]	17.9±1.8
Shear failure strain, γ_f [%]	43.9±3.4
Toughness in tension, G_{IC} [N/mm]	0.43±0.02
Toughness in shear, G_{IIC} [N/mm]	4.70±0.34

[a] manufacturer's data

[b] estimated from the Hooke's law using E and ν

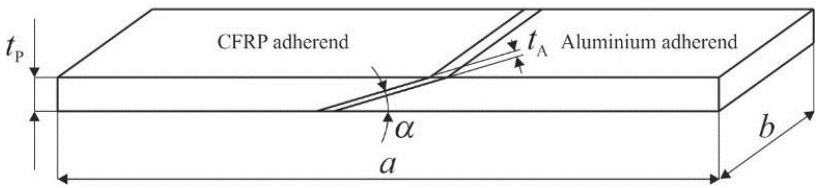

Figure 1 – Geometry and characteristic dimensions of the hybrid scarf joints.

Figure 1 shows the scarf joint geometry. The joint parameters are (in mm): joint length between gripping points, a=200, t_A=0.2, joint/adherend thickness, t_P=3, joint width, b=25 and α=10°, 15°, 20°, 30° and 45°. As for the adherends preparation, the aluminium adherends were cut from long bars supplied by the manufacturer, already with the final b. The tapered edges of these adherends were achieved by milling. On the other hand, for the composite adherends, the fabricated plates were initially cut in a table with an automated disc saw, while the tapered edges were then grinded with mounted points. For both adherend types, the bonding surfaces were roughened with sandpaper and cleaned with acetone. Bonding was then undertaken. Then, the joints were cured and the excess adhesive trimmed by milling processes. The tests were performed in a Shimadzu-Autograph AG-X testing equipment using a load cell with capacity of 100 kN, considering room temperature and humidity. The testing velocity was 1 mm/min for all specimens.

3. Numerical work

3.1. Numerical conditions

The FE simulations were performed in the commercial software Abaqus® accordingly to the following considerations. The aluminium adherends were modelled as continuum elements and considered as plastic isotropic, taking into consideration the elasto-plastic curve defined in reference [13]. The composite adherends, due to the absence of plasticization in the experimental tests, were modelled as elastic orthotropic elements and the mechanical properties are presented in reference [9]. The adhesive layer was modelled as a single row of cohesive elements connected to both the adherends, with a triangular traction-separation law (defined further in Section 3.2). For damage initiation and propagation, mixed-mode coupling criteria available in the Abaqus® software were used (stress-based for damage initiation and energy-based for damage propagation). According to the specimens' geometry depicted in Figure 1, a two-dimensional (2D) and plane-strain FE analysis is applicable for this work. **Error! Reference source not found.** presents an example of the mesh used at the bonded region, for the case of α=10º. This mesh was built by initiating the partitions of the adhesive layer along its length in blocks with a length of 0.1 mm, with each block representing one cohesive element. Taking into account the described procedure, the total number of cohesive elements used to model the adhesive layers' increases with the α reduction. The adherends partitions initiated from

those of the adhesive layer, and were transformed onto vertical and horizontal lines providing a complete structured mesh without any distorted elements. In the regions where large stress gradients are not expected, larger sized elements were used. For the construction of the FE mesh, 4 node plane-strain solid elements with reduced integration were considered (CPE4R elements available in Abaqus®), with exception of the scarf adherends' boundary elements. For this case, 3 node plane-strain solid elements (CPE3) were used. Cohesive elements with 4 nodes were applied in the adhesive layer (COH2D4).

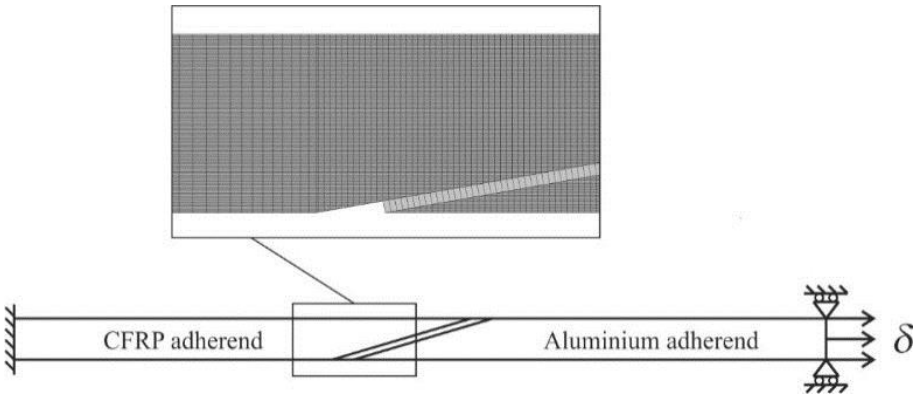

Figure 2 – Mesh detail and boundary conditions for a joint model with α=10º.

In order to replicate the real gripping conditions of the experimental tests, the following boundary conditions were considered: one of the specimen's edge was clamped while the other edge was pulled in tension while being restrained in the orthogonal direction, as shown in **Error! Reference source not found.**.

3.2. CZM description

Relationships among stresses and relative displacements linking similar nodes of cohesive elements are the fundament of the CZM. Additionally, those relations (often entitled CZM laws) may be established in pure and mixed mode and make possible to capture the material's behaviour up to failure [14]. This study relies on triangular pure and mixed-mode laws to model the adhesive layer. Under pure-mode loading, damage initiation occurs when the cohesive strength in tension or shear (t_n^0 or t_s^0, respectively) is attained, i.e., the material's elastic behaviour is cancelled and degradation starts [15]. Furthermore, the crack propagates up to the adjacent pair of nodes when the values of current tensile or shear cohesive stresses (t_n or t_s, respectively) become null. Under mixed-mode loading, stress and/or energetic criteria are often used to combine the pure-mode laws, and damage begins when the mixed mode cohesive strength (t_m^0) is reached [16]. Several criteria are available for damage initiation and growth when the analysis encompasses mixed-mode loadings. Nevertheless, this study focused on the quadratic nominal stress criterion and a linear power law form for the damage initiation and growth, respectively. This model is described in detail in the work of Rocha and Campilho [17]. The adhesives' properties used in Abaqus® are depicted in Table 1.

4. Results

4.1. Failure modes

After the tests performed, pictures were taken in order to study the failure mode of the samples, showing in all cases cohesive failure within the adhesive layer. Figure 3 shows two examples of experimental fractured surfaces, for joints bonded with Araldite® 2015, and α=10º (a) and α=45º (b).

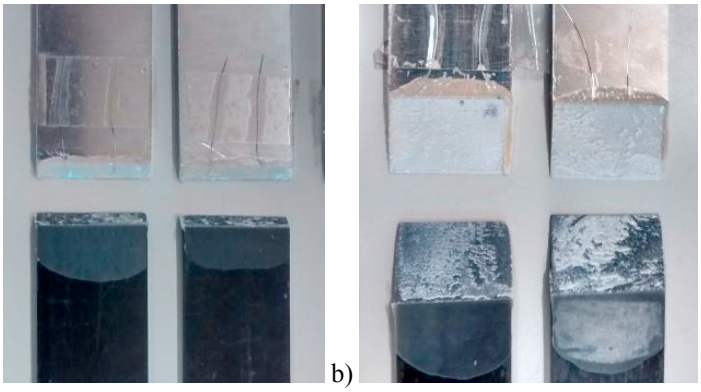

Figure 3 – Experimental failures for the joints with α=45º (a) and α=10º (b).

The CZM models were built considering the scarf joints modelled as perfectly bonded, with possibility of cohesive failure of the adhesive. After analysing all α, failure always began at the bond edges. However, damage in some geometries was a little bit higher near to x/L_S=1 compared to x/L_S=0, because of the lack of symmetry in the stress distributions, arising from the different adherends, as will be further discussed in this paper. Further loading the sample resulted in damage growth to the inner overlap until complete failure of the adhesive layer's CZM elements.

4.2. Stress analysis

All the graphics shown here were normalized by dividing σ_y and τ_{xy} by τ_{avg}, in which τ_{avg} represents the average τ_{xy} stress in the adhesive layer. The x-axis position was also normalized using the scarf length (L_S), such that x/L_S is considered, with $0 \leq x \leq L_S$. Figure 4 presents σ_y/τ_{avg} and τ_{xy}/τ_{avg} along the bondline as a function of α. All stress plots are asymmetric with respect to the middle of the adhesive layer (x/L_S=0.5), which opposes to the symmetric stress graphs for joints with similar adherends [18]. Both adherends have different stiffness, which causes stress asymmetry, consequently causing higher peak stresses at the scarfed tip of the composite adherend, because the stiffness of the composite is higher than that of the aluminium.

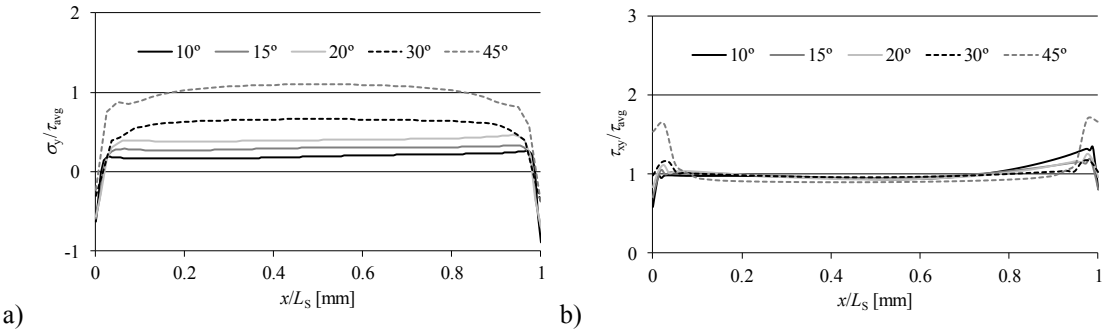

Figure 4 – σ_y (a) and τ_{xy} (b) stresses for the hybrid scarf joints at the adhesive mid-thickness.

Regarding σ_y stresses, the advantage of scarf joints, when comparing with single-lap joints, is that σ_y stresses show, irrespectively of α, small stress variations along the bondline [19]. This optimized behaviour is related to the tapered geometry of the adherends at the overlap [18]. By comparing different α, it can be concluded that higher α promote an increase of the σ_y/τ_{avg} peak stresses, up to attaining $\sigma_y/\tau_{avg} \approx 1$ for α=45º. Under these geometrical conditions, σ_y and τ_{xy} stresses are comparable. Actually, the maximum σ_y/τ_{avg} was equal to 1.10. Comparing this value with typical single-lap joints, much reduced peak stresses are present, which results in a higher joint performance. τ_{xy} stresses have the same asymmetric behaviour of σ_y stresses as previously described. Equally, the asymmetric plots are due to the

stiffness difference between adherends, which makes the adherends' longitudinal deformations different and induces a higher shear-lag effect. Oppositely, in non-hybrid joints, the results are symmetrical [18]. The lack of symmetry arises from the difference of longitudinal strain between the adherends at the overlap, which occurs because of the different adherends' stiffness. This promotes a higher shearing in the adhesive layer at the scarfed tip of the composite adherend. Despite these effects, τ_{xy} stresses possess a nearly uniform behaviour in the bondline. When the scarf geometry has α=45º, the gradient of τ_{xy}/τ_{avg} stresses is highest, and it is possible to observe a significant reduction for smaller α. In this case, τ_{xy} stresses attain a peak 1.70 times higher than τ_{avg}. This corresponds to a better performance when comparing with lap joints, because this joint presents a progressive t_P reduction at the bondline. Thus, the differential straining effect, preponderant in lap joints, is reduced [13]. The described behaviour of τ_{xy}/τ_{avg} stresses, combined with σ_y/τ_{avg} stresses, should result in higher strengths when compared with lap joints. Moreover, this should be particularly evident in joints with brittle adhesives, which cannot deal with peak stresses.

4.3. Experimental joint strength

The experimental maximum load (P_m) for the hybrid scarf joints bonded with Araldite® 2015 as a function of α is presented in Figure 5, showing that P_m increases exponentially with the α reduction. The improvement averaged over the scarf joint with α=45º was 30.3, 89.3, 136.9 and 231.7% for decreasing α between 30º and 10º. For adherends made of same material, a larger number of works corroborates this behaviour, which is caused by the corresponding exponential increase of the adhesive layer's length and advantage on stress distributions for smaller α [18].

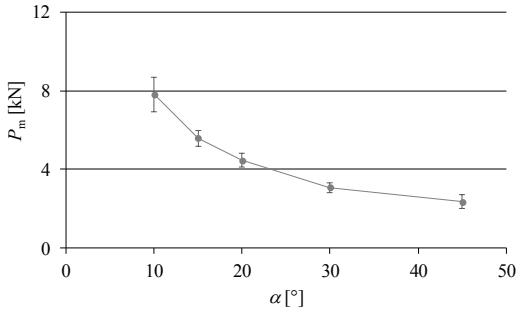

Figure 5 – Experimental P_m-α plot for the hybrid scarf joints.

In scarf joints with equal adherends, σ_y stresses decrease in relation to τ_{xy} stresses with the α reduction, while τ_{xy} peak stresses monotonically decrease at the same time. For mismatched adherends, the behaviour is similar for σ_y stresses. On the other hand, τ_{xy} stresses reduced between α=45º and α=30º, but they increased by further reducing α. Despite this fact, σ_y and τ_{xy} stresses have better performance for small α, which results in the corresponding increase of P_m (Figure 5). The standard deviation of the P_m values for each α is acceptable. The maximum percentile deviation was 14.7% for α=45º although, in absolute values, as it is clear from Figure 5, the standard deviation is much higher for smaller α. It is noteworthy that, even with α=10º, and considering σ_e of the aluminium alloy, P_m is only about 39.8% of this value. Considering σ_f instead of σ_e of the aluminium alloy, P_m can reduce for approximately 32.1%. Thus, full restitution of the parent structure's strength was not accomplished for the tested α.

4.4. Numerical strength prediction

The P-δ curves obtained from the numerical simulations revealed an abrupt failure after P_m. This behaviour is linked to the limited ductility of the chosen adhesive, and also due to the typical development of stresses along the bondline, with small variations, which normalizes the damage state along the adhesive [18]. A good agreement was found between the CZM P_m predictions and the test results of the hybrid joints, as shown in Figure 6.

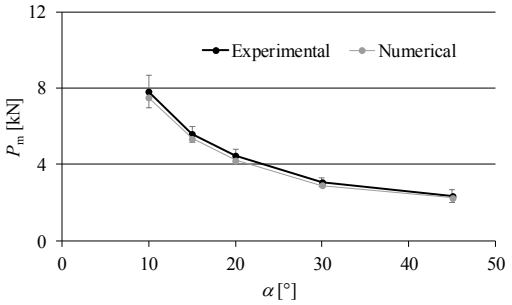

Figure 6 – Numerical P_m predictions for the hybrid scarf joints.

Between all tested α, the highest offset between both curves, averaged over the experimental curve, was of -5.3%, attained with α=30º. Moreover, the CZM P_m points are always inside the region defined by the experimental deviation, with preponderance of numerical points below the experimental data points. Although this is not a major issue for the limited ductility of the adhesive being tested, this may be related to the consideration of a triangular CZM to model an adhesive that has a non-negligible plastic portion in its σ-ε curve. Under these conditions, before P_m is attained in the hybrid joints, the adhesive suffers some plastics deformations, and this effect is not accurately captured by the bilinear CZM, because it promotes the reduction of transferred stresses when t_m^0 is reached. This then translates into a smaller amount of loads being transferred at this regions, and can artificially reduce P_m.

4.5. Numerical assessment of the adherends' material

After the successful validation of the CZM technique, a purely numerical study is conducted that evaluates the hybrid joint P_m performance compared with purely aluminium and CFRP joints. Figure 7 gives the variable Δ [%] as a function of α, which gives the % P_m variation measured between joints with both adherends made of aluminium or CFRP adherends and the hybrid joints addressed in the former Section, normalized to the hybrid results.

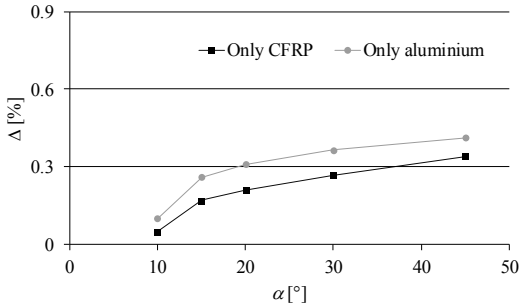

Figure 7 – Percentile P_m variation (Δ [%]) between the balanced joints and the hybrid joints.

The figure shows that always Δ [%] > 0. Thus, having an adherend-balanced joint always yields better results. This is a concept that can be closely related to the σ_y and τ_{xy} stress distributions: using equal adherends, both stress components are symmetric, leading to a peak stress reduction [20]. The highest Δ was 0.41%, for a joint with aluminium adherends and α=45º. It is expected that the type of adhesive, especially the ductility (accounted by G_{IC} and G_{IIC}), highly influences Δ. For example, a brittle adhesive does not deal well with peak stresses. Thus, by balancing the adherends, a higher Δ is expected than when considering adhesives with some ductility.

5. Conclusions

This work aimed at experimental and numerically studying hybrid scarf joints. The analysis was supported by a σ_y and τ_{xy} stress analysis, which highlighted the asymmetry of the stress plots due to the distinct axial stiffness between mismatched adherends. σ_y stresses were mostly flat, although with increasing relative importance compared to τ_{xy} stresses, as α increased. τ_{xy} stresses had the highest peak stresses in the scarf joints with α=45º, even though this effect was very limited in extent. The P_m-α plot showed an exponential increase of P_m by reducing α. This behaviour was found because of the corresponding increase of bonded length with smaller α, and better stress distributions. The numerical results showed good P_m predictions, with a maximum relative offset of -5.3% for α=30º. Moreover, it was found that the numerical P_m were always below the average P_m obtained in the tests. The purely numerical study that compared the hybrid joints' results with those of joints with balanced adherends revealed a minimal difference in P_m, but always with advantage with balanced adherends. As a final conclusion, this work detailed the failure process of hybrid adhesive joints, and proposed and validated the CZM technique for design purposes.

References

[1] E.M. Petrie. Handbook of adhesives and sealants. New York: McGraw-Hill; 2000.
[2] H. Dannbauer, C. Gaier, K. Hofwimmer. Fatigue Analysis of Welding Seams and Spot Joints in Automotive Structures. SAE International; 2005.
[3] D.P. Graham, A. Rezai, D. Baker, P.A. Smith, J.F. Watts, The development and scalability of a high strength, damage tolerant, hybrid joining scheme for composite–metal structures, Composites Part A: Applied Science and Manufacturing, 64 (2014) 11-24.
[4] A. Kimiaeifar, H. Toft, E. Lund, O.T. Thomsen, J.D. Sørensen, Reliability analysis of adhesive bonded scarf joints, Engineering Structures, 35 (2012) 281-7.
[5] M. Afendi, T. Teramoto, H.B. Bakri, Strength prediction of epoxy adhesively bonded scarf joints of dissimilar adherends, International Journal of Adhesion and Adhesives, 31 (2011) 402-11.
[6] V.D. Yelpale, S.M. Jadhao, M.S. Kamble, Strength Evaluation of Scarf Adhesive Joints with Different Adherends Subjected to Static Tensile Loading, International Journal of Innovative Research in Science, Engineering and Technology, 5 (2016) 12258-63.
[7] ASTM-E8M-04. Standard test methods for tension testing of metallic materials [Metric]. West Conshohocken, PA: ASTM International; 2004.
[8] R.D.S.G. Campilho, M.D. Banea, A.M.G. Pinto, L.F.M. da Silva, A.M.P. de Jesus, Strength prediction of single- and double-lap joints by standard and extended finite element modelling, International Journal of Adhesion and Adhesives, 31 (2011) 363-72.
[9] F.M.F. Ribeiro, R.D.S.G. Campilho, R.J.C. Carbas, L.F.M. da Silva, Strength and damage growth in composite bonded joints with defects, Composites Part B: Engineering, 100 (2016) 91-100.
[10] R.D.S.G. Campilho, M.D. Banea, J.A.B.P. Neto, L.F.M. da Silva, Modelling adhesive joints with cohesive zone models: effect of the cohesive law shape of the adhesive layer, International Journal of Adhesion and Adhesives, 44 (2013) 48-56.
[11] A.C.C. Leitão, R.D.S.G. Campilho, D.C. Moura, Shear Characterization of Adhesive Layers by Advanced Optical Techniques, Experimental Mechanics, 56 (2016) 493-506.
[12] R.D.S.G. Campilho, D.C. Moura, D.J.S. Gonçalves, J.F.M.G. da Silva, M.D. Banea, L.F.M. da Silva, Fracture toughness determination of adhesive and co-cured joints in natural fibre composites, Composites Part B: Engineering, 50 (2013) 120-6.
[13] S.L.S. Nunes, R.D.S.G. Campilho, F.J.G. da Silva, C.C.R.G. de Sousa, T.A.B. Fernandes, M.D. Banea, et al., Comparative failure assessment of single and double-lap joints with varying adhesive systems, The Journal of Adhesion, 92 (2016) 610-34.
[14] H. Luo, Y. Yan, T. Zhang, Z. Liang, Progressive failure and experimental study of adhesively bonded composite single-lap joints subjected to axial tensile loads, Journal of Adhesion Science and Technology, 30 (2016) 894-914.
[15] A.U. Sane, P.M. Padole, C.M. Manjunatha, R.V. Uddanwadiker, P. Jhunjhunwala, Mixed mode cohesive zone modelling and analysis of adhesively bonded composite T-joint under pull-out load, Journal of the Brazilian Society of Mechanical Sciences and Engineering, 40 (2018) 167.
[16] R. Dimitri, M. Trullo, L. De Lorenzis, G. Zavarise, Coupled cohesive zone models for mixed-mode fracture: A comparative study, Engineering Fracture Mechanics, 148 (2015) 145-79.
[17] R.J.B. Rocha, R.D.S.G. Campilho, Evaluation of different modelling conditions in the cohesive zone analysis of single-lap bonded joints, The Journal of Adhesion, (2017) in press.
[18] R.D.F. Moreira, R.D.S.G. Campilho, Strength improvement of adhesively-bonded scarf repairs in aluminium structures with external reinforcements, Engineering Structures, 101 (2015) 99-110.
[19] M. Davis, D. Bond, Principles and practices of adhesive bonded structural joints and repairs, International Journal of Adhesion and Adhesives, 19 (1999) 91-105.
[20] R.A. Odi, C.M. Friend, An improved 2D model for bonded composite joints, International Journal of Adhesion and Adhesives, 24 (2004) 389-405.